The Astrophysical Journal, 833:112 (9pp), 2016 December 10 doi:10.3847/1538-4357/833/1/112

GAS FRACTION AND DEPLETION TIME OF MASSIVE STAR-FORMING GALAXIES AT $z \sim 3.2$: NO CHANGE IN GLOBAL STAR FORMATION PROCESS OUT TO $z > 3$

E. Schinnerer[1], B. Groves[2], M. T. Sargent[3], A. Karim[4], P. A. Oesch[5,6], B. Magnelli[4], O. LeFevre[7], L. Tasca[7], F. Civano[8,9], P. Cassata[10], and V. Smolčić[11]

[1] Max Planck Institute for Astronomy, Königstuhl 17, D-69117 Heidelberg, Germany
[2] Research School of Astronomy and Astrophysics, Australian National University, Canberra, ACT 2611, Australia
[3] Astronomy Centre, Department of Physics and Astronomy, University of Sussex, Brighton, BN1 9QH, UK
[4] Argelander-Institut für Astronomie, Universität Bonn, Auf dem Hügel 71, D-53121 Bonn, Germany
[5] Yale Center for Astronomy and Astrophysics, Department of Physics and Astronomy, Yale University, New Haven, CT 06511, USA
[6] Observatoire de Geneve, Geneva University, 51 Ch. des Maillettes, 1290 Versoix, Switzerland
[7] Aix-Marseille Université, CNRS, LAM (Laboratoire d'Astrophysique de Marseille) UMR 7326, F-13388 Marseille, France
[8] Yale Center for Astronomy and Astrophysics, 260 Whitney Avenue, New Haven, CT 06520, USA
[9] Harvard-Smithsonian Center for Astrophysics, 60 Garden Street, Cambridge, MA 02138, USA
[10] Instituto de Fisica y Astronoma, Facultad de Ciencias, Universidad de Valparaiso, 1111 Gran Bretana, Playa Ancha Valparaso, Chile
[11] Department of Physics, University of Zagreb, Bijenička cesta 32, HR-10000 Zagreb, Croatia

Received 2016 June 10; revised 2016 October 6; accepted 2016 October 11; published 2016 December 12

ABSTRACT

The observed evolution of the gas fraction and its associated depletion time in main-sequence (MS) galaxies provides insights on how star formation proceeds over cosmic time. We report ALMA detections of the rest-frame ~300 μm continuum observed at 240 GHz for 45 massive ($\langle \log(M_\star(M_\odot)) \rangle = 10.7$), normal star-forming ($\langle \log(\mathrm{sSFR}(\mathrm{yr}^{-1})) \rangle = -8.6$), i.e., MS, galaxies at $z \approx 3.2$ in the COSMOS field. From an empirical calibration between cold neutral, i.e., molecular and atomic, gas mass M_{gas} and monochromatic (rest-frame) infrared luminosity, the gas mass for this sample is derived. Combined with stellar mass $M_\star$ and star formation rate (SFR) estimates (from MAGPHYS fits) we obtain a median gas fraction of $\mu_{\mathrm{gas}} = M_{\mathrm{gas}}/M_\star = 1.65^{+0.18}_{-0.19}$ and a median gas depletion time $t_{\mathrm{depl.}}(\mathrm{Gyr}) = M_{\mathrm{gas/SFR}} = 0.68^{+0.07}_{-0.08}$; correction for the location on the MS will only slightly change the values. The reported uncertainties are the 1σ error on the median. Our results are fully consistent with the expected flattening of the redshift evolution from the 2-SFM (2 star formation mode) framework which empirically prescribes the evolution assuming a universal, log-linear relation between SFR and gas mass coupled to the redshift evolution of the specific star formation rate (sSFR) of MS galaxies. While $t_{\mathrm{depl.}}$ shows only a mild dependence on location within the MS, a clear trend of increasing μ_{gas} across the MS is observed (as known from previous studies). Further, we comment on trends within the MS and (in)consistencies with other studies.

Key words: galaxies: evolution – galaxies: high-redshift – galaxies: ISM – submillimeter: ISM

1. INTRODUCTION

Knowledge of the gas fraction and depletion time of galaxies beyond the peak epoch of cosmic star formation rate (SFR) density, i.e., at redshifts $z > 2$ is critical to determine their main mode of star formation and the efficiency of the star formation process. The study of galaxies in this redshift range is especially interesting in the context of potential discrepancies between the relative shape of the dark matter halo gas accretion rate and the measured evolution of the specific star formation rate (sSFR). For example, comparison between observations and predictions from cosmological simulations can test how efficiently accreted gas is incorporated into the gaseous disks and converted to stars, e.g., gas fractions are fairly sensitive to the prescription used for the conversion of cold gas into stars (see the recent review by Somerville & Davé 2015).

The evolution of the gas fraction and depletion time beyond $z \sim 2.5$ is currently less well constrained than at lower redshifts (e.g., the recent compilation by Genzel et al. 2015), as fewer objects have had their cold gas fraction measured. Studies so far have focused on small samples consisting of lensed galaxies (e.g., Saintonge et al. 2013; Dessauges-Zavadsky et al. 2015) and non-lensed objects (Magdis et al. 2012; Tan et al. 2014) for direct detections. Normal star-forming galaxies are observed to form a tight relation in the SFR versus stellar mass plane which is often referred to as the "main sequence" (MS) of star-forming galaxies (Noeske et al. 2007) whose normalization is a strong function of redshift (for recent determinations at our redshift range of interest, see, e.g., Tasca et al. 2015). Recently, Bethermin et al. (2015) extended the analysis to $z = 4$ using infrared stacking and Scoville et al. (2016) presented the first direct measurements for galaxies on and off the MS out to $z \approx 4.4$. These studies provide the first important constraints on the gas fraction and depletion time, suggesting that star formation in MS galaxies, i.e., normal star-forming galaxies, proceeds in a fashion similar to low-redshift galaxies.

Probing the cold or molecular gas mass directly for $z > 3$ MS galaxies is very challenging even in the era of ALMA, as the expected strength of the CO emission lines requires long integration times. Furthermore, ALMA can typically only access high-J transitions (CO(3-2) is the lowest transition accessible for such sources) which are more prone to excitation effects and their relation to the bulk amount of molecular gas present is less straightforward (see, e.g., Carilli & Walter 2013). The only possibility to quickly assemble sizable samples is to use the large bandwidth available for continuum detections and rely on the observed tight relation between cold dust mass and neutral (i.e., molecular and atomic) gas mass (e.g., Hildebrand 1983). This gas-to-dust ratio technique can either use the full information from the infrared spectral energy distribution or rely on a direct, locally calibrated relation between the sub-

millimeter dust continuum and the cold gas mass (e.g., Magnelli et al. 2014; Scoville et al. 2014; Groves et al. 2015). In general this method seems to lead to results that are in good agreement with CO-based gas masses (Genzel et al. 2015) and has become increasingly popular (Magdis et al. 2012; Magnelli et al. 2014; Santini et al. 2014; Scoville et al. 2014, 2016; Bethermin et al. 2015). Both methods (via the CO line or dust continuum) rely on local calibrations and thus exhibit a dependency on metallicity. Therefore, studies of high-redshift galaxies, particularly on the low-mass end, can be significantly affected by our ability to measure or statistically infer gas phase metallicities (e.g., Bethermin et al. 2015).

The sample, its properties, and the data used for their determination are described in Section 2. The gas mass estimation and results on the gas fraction and depletion time are presented in Section 3 and discussed in Section 4. We summarize and conclude in Section 5. Throughout the paper we assume a cosmology with $H_0 = 70$, $\Omega_M = 0.3$ and $\Omega_\Lambda = 0.7$ (for ease of comparison to other work in the literature) and use a Chabrier initial mass function for the stellar mass and SFR determination.

2. SAMPLE AND DATA

2.1. Sample Selection

To study the cold gas fraction and the gas depletion time at a redshift of $z \sim 3$–4, we selected a sample of massive star-forming galaxies in the COSMOS field to be observed with ALMA. Our initial sample selection is based on the phot-z catalog of Ilbert et al. (2013) selecting all sources with good phot-z estimates ($\Delta z < \pm 0.2$) in the range $z_{\rm phot} = 3.0$–4.0 and masses determined by LePhare (Arnouts et al. 1999, 2002; Ilbert et al. 2006) with $\log(M_\star [M_\odot]) > 10.5$ (corresponding to UltraVISTA magnitudes of $K_s \lesssim 23$ mag (McCracken et al. 2012)). To select star-forming galaxies, we cross-matched our sample with the Muzzin et al. (2013) catalog and selected all objects with a MIPS 24 μm counterpart of $\sim 3\sigma$ in the Muzzin et al. (2013) catalog and with standard rest-frame UV–optical colors expected for star-forming systems (based on the $J - [4.5]$(IRAC2) color versus M_z). This selection resulted in 73 sources. We added an additional 13 objects with spectroscopic redshifts in our redshift and stellar mass range from a preliminary analysis of the VIMOS Ultra Deep Survey (VUDS, LeFevre et al. 2015) that matched our star-forming requirements, resulting in a total of 86 potential target galaxies.

For the analysis presented here we updated the photometry and redshift determination of this initial sample based on the COSMOS2015 catalog of Laigle et al. (2016). This catalog includes new $YJHK_s$ imaging from the UltraVISTA DR2 release, Y-band imaging from Hyper Suprime-Cam and deeper SPLASH data at 3.6 and 4.5 μm (SPitzer Large Area Survey, PI: Capak; Steinhardt et al. 2014). The photometric redshifts are determined using the template-fitting LePhare code based on the updated photometry using the fluxes computed within 3″ apertures. (Furthermore, we remeasured the MIPS 24 μm and PACS 100 μm fluxes; see Section 2.3 for details.)

For 22 sources of our initial sample, spectroscopic redshifts with high quality (flag $\geqslant 2$, $>75\%$ probability of being correct) exist to date, 15 from VUDS (LeFevre et al. 2015) and 7 sources mainly from zCOSMOS-deep (Lilly et al. 2007). For these sources we use the spectroscopic redshifts instead of the photometric ones, which are consistent in all but two cases. With these new redshifts, 7 of our original 86 sources have $z < 2.8$. Excluding these sources, the median redshift of our sample is $z = 3.2$ with the highest redshift being $z = 3.8$.

2.2. ALMA Data

The 86 target fields were observed as part of an ALMA Cycle 2 program (2013.1.00151.S, PI: Schinnerer). The observations were optimized for continuum detections at 240 GHz (corresponding to $\sim$300 μm rest-frame at the median sample redshift of $z = 3.2$) using the correlator in TDM mode with the four spectral windows centered at 231, 233, 247, and 249 GHz yielding a total bandwidth of 7.5 GHz. The target fields were observed with typically 38 antennas between 2014 December 25 and 30 for a total of 2.0 minutes on-source integration time, with 24 fields receiving an additional 0.5 minutes on-source time. The quasar J1010-0200 served as phase calibrator in all observations; for bandpass and flux calibration J1058+0133, J0750+1231, J0854+201, J0825+0309, J1037-295, Ganymede, and Callisto were observed. We used the calibrated data products provided by the ALMA project. The resolution and rms achieved is $1\farcs8 \times 1\farcs1$ ($1\farcs7 \times 1\farcs1$) and 66 (71) μJy/beam for the 24 (62) fields with (without) additional observing time when using natural weighting. We CLEANed all four spectral windows together using the "mfs" mode down to 3σ without setting a CLEAN box and using up to 1000 iterations. The final images cover an area of $39'' \times 39''$ with a pixel size of $0\farcs18$ sufficient to encompass the primary beam FWHM of 23″ at 240 GHz.

2.3. Stellar Mass and SFR Estimation

Due to the updated redshift information for about 25% of our objects and the better photometry available, we re-determined the stellar mass and SFR for each ALMA target. Given the expected large amounts of gas and dust present in our targets, we cannot rely on the UV emission alone to estimate the SFR due to the large, uncertain correction factors required. For all objects, 24 and 100 μm fluxes or upper limits were extracted from the *Spitzer*/MIPS 24 μm map from Le Floc'h et al. (2009) and the *Herschel*/PACS 100 μm image from Lutz et al. (2011) using the PSF-fitting method of Magnelli et al. (2013) to simultaneously search for emission associated with the position of our targets, while also accounting for the flux from all known 24 μm sources around it. This careful de-blending is in particular necessary for sources #26250, #26318, and #26388 as well as #226676 and #226748 which lie close together (within $\sim 10''$, but still apart at 24/100 μm resolution). This resulted in a significant fraction ($\sim$30%) of targets without 3σ MIPS 24 μm detections irrespective of the source being ALMA detected or not. Only six sources are detected in the PACS 100 μm image above 3σ; half of these are detected by ALMA as well. This low detection rate is consistent with the depth of the PACS 100 μm image and the anticipated SFR of our targets.

Stellar masses and SFRs for the full sample are determined by fitting the available photometry within a 3″ aperture (from the catalog of Laigle et al. 2016), including our measured IR +ALMA fluxes and assuming the best available redshifts, with the MagPhys code (da Cunha et al. 2008).[12] Non-detections

[12] In particular, we use the Bruzual & Charlot (2003) stellar libraries and the latest "high-z" version of the code available at http://www.iap.fr/magphys/magphys/ MAGPHYS.html.

by ALMA (see Section 3.1) are treated as upper limits. All PACS 100 μm photometry are also used as upper limits due to their low signal-to-noise ratio (S/N) ($<5\sigma$ in case of the non-detections) and potential confusion due to their low resolution. The MIPS 24 μm data photometry was excluded from the fitting due to the highly uncertain SEDs for star-forming galaxies and potential contribution from an AGN.

Stellar masses determined with MAGPHYS are consistent (barring a systematic 0.2 dex offset) with LEPHARE-based estimates in Laigle et al. (2016) for 90% of the sample, and are independent (within uncertainty) of the inclusion of the IR +ALMA data. Both UV and IR fluxes are used for our SFR measurements. When IR+ALMA photometry is excluded, SFRs are lowered by 0–0.5 dex, indicating that significantly obscured star-forming regions play a role in several of our sources. The use of the Bayesian SED-fitting code MAGPHYS allows us to include both these buried populations as well as the uncertainty of the IR SED which is mainly constrained by the PACS 100 μm upper limits and ALMA data points. We remind the reader that the optical/NIR data also provide a constraint through the rest-frame UV–optical shape to indicate possible extinction as indicated by the small offset mentioned above between the fits with and without the inclusion of the IR +ALMA data (though extremely heavily obscured young stellar populations are only constrained by the IR SED). We verified that our average SFR is consistent with the mean and median SFR determined from the stacked IR SED (see Section 3.1). Moreover, the resulting average SED obtained via MAGPHYS agrees very well with the stacked SED. While the SFRs of individual sources will suffer from the usual (systematic) uncertainties that are unavoidable for sources with poor sampling of their rest-frame infrared to sub-millimeter SED, the average SFR of our sample is hence robustly determined.

We have also identified 12 possible AGNs in our sample by cross-matching with the *Chandra* COSMOS Legacy survey (Civano et al. 2016) and through a mid-IR excess (i.e., red [4.5]–[5.8] and [5.8]–[8.0] colors, e.g., following the methodology of Lacy et al. 2007). Mid-IR excess AGNs were identified via offsets in the IRAC photometry (in particular at 8 μm) compared to the fitted MAGPHYS SED, which could not be reproduced by any reasonable stellar SED. Two sources have clear (e.g., S/N > 5) X-ray detections, while six more have weak X-ray detections, which we also classify as AGNs. Seven sources have noticeable IR excesses, three of which also have X-ray detections.

In Figure 1 we show the location of our $z \sim 3.2$ sample in the SFR versus $M_\star$ plane with respect to the location of the "MS" of star-forming galaxies at redshift $z \approx 3$ (Lee et al. 2010; Magdis et al. 2010; Bethermin et al. 2014; Heinis et al. 2014; Schreiber et al. 2015; Tasca et al. 2015; Tomczak et al. 2016).[13] Our ALMA detections sample the MS at high stellar mass ($\log(M_\star[M_\odot]) \approx 10.3$–$11.5$) and are not biased toward a particular SFR range ($\log(\mathrm{SFR}[M_\odot\ \mathrm{yr}^{-1}]) \approx 1.5$–$3$).

[13] In the compilation of MSs used by the 2-SFM framework (Sargent et al. 2014) and updated with recent sSFR measurements (Bethermin et al. 2014; Heinis et al. 2014; Steinhardt et al. 2014; Schreiber et al. 2015; Tasca et al. 2015), galaxies with stellar masses of $\log(M_\star[M_\odot]) \approx 10.7$ (the typical mass of our sample galaxies) show no evidence for an evolution of their sSFR values for $3 \leqslant z \leqslant 4$ and have an average sSFR of $\sim 3\ \mathrm{Gyr}^{-1}$ with an rms dispersion of 0.13 dex. This is in good general agreement with other sSFR compilations (e.g., by Speagle et al. 2014).

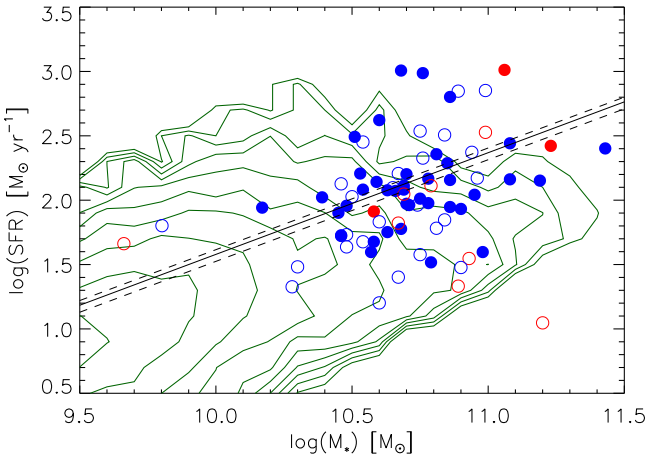

Figure 1. Location of our $z > 2.8$ ALMA targets (detections: filled circles; non-detections: open circles) in the SFR vs. stellar mass $M_\star$ plane compared to the distribution of all galaxies with good photometric redshifts at $z \approx 2.8$–4.0 in the COSMOS field (contours; $M_\star$ and SFR (both based on LEPHARE) are taken from Laigle et al. (2016)). The solid line marks the location of the main sequence of star-forming galaxies at $z = 3.2$ (dashed lines correspond to $z = 2.8$ and 3.6, respectively) based on Sargent et al. (2014). AGNs are highlighted in red (see the text for details).

3. RESULTS

3.1. 240 GHz Continuum Detection and Gas Mass Measurements

For the detection of sources in our 86 target fields we use the source extraction software of Karim et al. (2013) which was developed for continuum-source extraction in ALMA imaging data. The software automatically identifies sources at $\geqslant 2.5\sigma$ and determines the flux based on a comparison of a three-parameter (assuming an unresolved source) and six-parameter (assuming a resolved source) Gauss fit in the image plane. A total of 47 of our 86 targeted sources are detected at or above 3σ (for the peak), with 45 (52%) lying at a redshift of $z > 2.8$. We use the integrated fluxes from the six-parameter fit and verified that it gives consistent results for unresolved sources. We further tested that Gaussian fits at the position of the optical/near-IR sources result in similar values. For the ease of comparison of serendipitous detections in our target fields in future work we use the values provided by the blind extraction software.

Based on the completeness tests done by Karim et al. (2013) up to 5% of our detected sources (corresponding to ~2 sources) could be spurious for a full sample of blind detections. Given that we are searching at predetermined positions, the probability is even lower, as our fields contain about 350 independent beams, so the chance that a spurious source would end up in the center is about 0.3% (if there is one source per field). The typical number of sources detected per field is about seven, thus there is a ~2% chance that such a source would end up at the position of our targeted objects. Therefore we are confident that all our detections are real.

To convert the observed 240 GHz flux density into a cold gas mass, we make use of the observed relation between cold dust luminosity and gas mass (similar to, e.g., Scoville et al. 2014, 2016). Recently, Groves et al. (2015) calibrated relations between monochromatic IR luminosities at 250, 350, and 500 μm and neutral (atomic plus molecular) gas mass using high-quality observations for 36 local galaxies from the KINGFISH survey (Kennicutt et al. 2011). These calibrations

implicitly include the effects of metallicity through the variation within the calibration sample. The calibration between monochromatic luminosity and gas mass becomes steeper and has larger scatter at shorter IR wavelengths because of the effect of dust temperature and its correlation with stellar mass and metallicity. Here we adopt the relations for the high-mass sample, i.e., $\log(M_\star) > 9.0$ at rest-frame 250 and 350 μm (see Table 6 of Groves et al. 2015) and linearly interpolate the coefficients to match the observed rest-frame wavelengths:

$$\log_{10}(M_{\rm gas}(M_\odot)) = (1.57 - 8 \times 10^{-4}\Delta\lambda) + (0.86 + 6 \times 10^{-4}\Delta\lambda) \times \log_{10}(\nu L_{\rm nu}(L_\odot)) \quad (1)$$

where

$$\Delta\lambda = \lambda_{\rm ALMA,restframe} - 250\ \mu{\rm m} \quad (2)$$

and

$$\nu L_\nu = \nu_{\rm obs} \times S_{\nu,\rm obs} \times 4\pi \times D_L^2. \quad (3)$$

As discussed by Groves et al. (2015) the monochromatic IR luminosity relations are similar to other methods advertised such as, e.g., the calibration of the 850 μm luminosity by Scoville et al. (2014, 2016). We verified that gas masses derived using the Scoville et al. (2014) prescription are consistent with our results within the (systematic) uncertainties. The metallicities of high-redshift galaxies are highly uncertain given the changes in the physical properties in these galaxies (see, e.g., Kewley et al. 2013, 2015). Thus we assume that the metallicities of massive galaxies at our epoch of interest are broadly consistent with local objects of similar masses. However, there are suggestions that the metallicities of massive galaxies have increased since $z \sim 3$ to now, with suggestions of around a factor of two (e.g., Maiolino et al. 2008; Troncoso et al. 2014; Onodera et al. 2016). If this is the case our determinations for the gas mass of our sample are likely underestimated (by approximately 0.3 dex), as we overestimate the metallicity and hence the dust-to-gas ratio in our detected sample. Note that the presumably higher dust temperature for galaxies at our redshifts (e.g., Bethermin et al. 2015; Genzel et al. 2015) compared to the local sample could counteract such a systematic trend.

As a further confirmation, we also derived the average gas mass of our detected sources in the redshift range $z = 2.8$–3.7 through determining the gas mass from stacking of the (*Spitzer* and *Herschel*) infrared data centered on our detected source positions. We use the methodology of Magnelli et al. (2014) as used for Genzel et al. (2015), i.e., a modified Draine & Li (2007) model is fitted to the IR data points plus the average 240 GHz ALMA flux density, providing a mean dust temperature and dust mass for the sample. The average dust mass obtained with this approach is then converted into a gas mass by applying the metallicity-dependent dust-to-gas ratio for $z \sim 0$ star-forming galaxies found by Leroy et al. (2011). The average metallicity of our detected sources is derived using the stellar-mass–metallicity relation at their average redshift as found in Genzel et al. (2015). Comparison of the average metallicity of our detection sample based on the Genzel et al. (2015) prescription (which uses the mass–metallicity relation of Maiolino et al. 2008) yields very similar results (within <0.1 dex) as more recent determinations of the mass–metallicity relation (e.g., Troncoso et al. 2014; Onodera et al. 2016).

The mean gas mass derived from the fit to the stacked infrared SED of $\langle M_{\rm gas}(M_\odot)\rangle_{\rm IRSED} = 10.89$ (with a full accounting of the potential effect of the mass–metallicity relation) is remarkably similar to the mean gas mass from the monochromatic approach of $\langle M_{\rm gas}(M_\odot)\rangle_{\rm L300} = 10.84$. We take this as an indication that no strong systematic biases are present between results from these two approaches when comparing the same high-mass objects.

For the subsequent analysis we restrict the sample to objects with ALMA detections in the redshift range of $z = 2.8$–3.7. These objects have a robust determination of their SFRs due to the inclusion of the ALMA fluxes, as our re-measuring of the IR photometry for all objects sometimes led to a significant change in the MIPS 24 μm flux. These 45 objects sample fairly well the SFR versus stellar mass $M_\star$ plane (see also Figure 1) and have a mean redshift of $z = 3.2$, a mean stellar mass of $\langle\log(M_\star[M_\odot])\rangle = 10.7$, and a mean SFR of $\langle\log({\rm SFR}[M_\odot\ {\rm yr}^{-1}])\rangle = 2.1$. The average specific SFR (sSFR) of our sample is $\log({\rm sSFR}[{\rm yr}^{-1}]) = -8.6$, so our sample lies close to the MS at the mean redshift of our sample (with a median offset of −0.04 dex, i.e., very slightly below the MS, but well within the MS scatter).

3.2. Gas Fraction and Gas Depletion Time

In the following we combine the estimates of stellar mass, SFR, and gas mass for our 45 detections at $2.8 \leqslant z < 4$ to study the evolution of the gas fraction, defined as $\mu_{\rm gas} = M_{\rm gas}/M_\star$, and gas depletion time, defined as $t_{\rm depl.} = M_{\rm gas}/{\rm SFR}$. We compare our measurements to lower redshift results available from the literature as well as empirical predictions for MS galaxies (at our target redshift) from the 2-SFM model (Sargent et al. 2014). The 2-SFM predictions are based on (a) a log-linear, redshift-independent star formation law (calibrated for $z < 2.5$ MS galaxies) relating SFR and molecular gas mass, and (b) the observed redshift evolution of the specific SFR of MS galaxies. We remind the reader that values derived for individual galaxies have significant uncertainties and might suffer from systematic uncertainties. However, given the independent cross-checks on the average properties done in Sections 2.3 and 3.1, we expect that average trends described in the following are robust.

3.2.1. Relevance of Being on the MS of Star-forming Galaxies

In Figure 2(a) we show the deviation of the measured gas fraction $\mu_{\rm gas}$ relative to the expected[14] gas fraction ($\mu_{\rm gas}/\langle\mu_{\rm gas}\rangle_{\rm MS}$) of a star-forming galaxy located exactly on the mean MS locus. Gas fractions are predicted (gray shaded areas in Figure 2) to vary significantly as a function of offset ${\rm sSFR}/\langle{\rm sSFR}\rangle_{\rm MS}$ from the MS. In keeping with expectations, we do see a trend in our data that galaxies below the MS, i.e., with lower SFR for a given stellar mass, exhibit a lower gas fraction while galaxies above the MS have a higher gas fraction. Over the range of specific SFR probed by our galaxies (±0.7 dex or from 20% to 500% of the MS value), their gas fractions range over 1.5 dex (from ∼20% to 600% of the average MS value). This trend is consistent with the 2-SFM

[14] Given the stellar mass of an average MS galaxy, its SFR is determined by the sSFR evolution of MS galaxies. The (molecular) gas mass of this galaxy is given by the trend line of the integrated $M_\star$–$M_{\rm gas}$ relation in Figure 5. The stellar and gas masses have then been combined to form the expected gas fraction$\langle\mu_{\rm gas}\rangle$ if a "typical" MS galaxy.

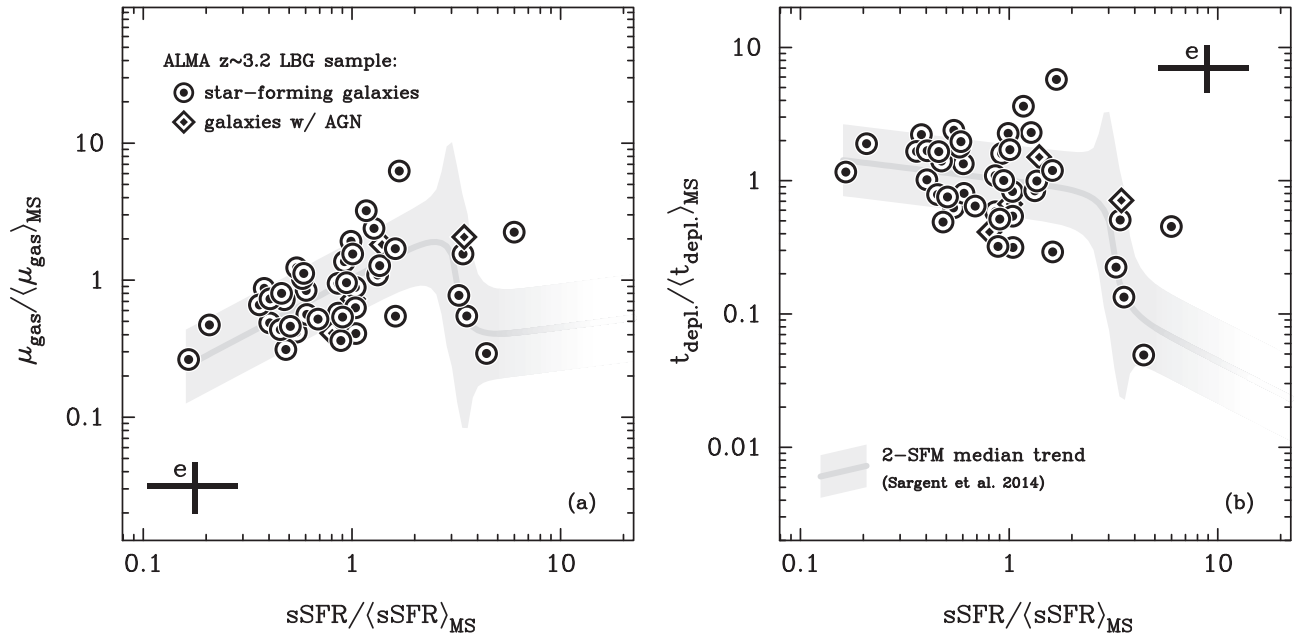

Figure 2. Gas fraction and depletion time vs. specific SFR (sSFR) of our $z = 3.2$ sample relative to average main-sequence properties. Left, panel (a): the gas fraction $\mu_{gas} = M_{gas}/M_{\star}$ relative to the average gas fraction of main-sequence galaxies $\langle\mu_{gas}\rangle_{MS}$ of our sample is shown as black symbols. Right, panel (b): the gas depletion time $t_{depl.} = M_{gas}/SFR$ relative to the average gas depletion time of main-sequence galaxies $\langle t_{depl.}\rangle_{MS}$ of our sample is presented by black symbols. Circles and diamonds indicate star-forming galaxies and candidate AGN hosts. The cross marked with "e" represents the typical error bars in each panel. It includes the scatter of sSFR measurements as reported in the literature, i.e., it also illustrates the systematic uncertainties relating to the exact normalization of the MS and also the best-fit Schmidt–Kennicutt relation. The dark gray line shows the predicted, redshift-invariant median trends from the 2-SFM framework Sargent et al. (2014) as a function of distance from the main sequence of star-forming galaxies (with the gray band spanning the expected 1σ scatter around the average). The gray coloring fades out toward the extreme starburst regime, which is not relevant to this study. Note that for low-z galaxies the contribution of atomic (H I) gas is not included in M_{gas}.

predictions, thus implying a close correlation between SFR and M_{gas} as observed in $z < 2.5$ galaxies.

A similar plot is shown for the deviation of the depletion time relative to the average depletion of the MS $t_{depl.}/\langle t_{depl.}\rangle_{MS}$ in Figure 2(b). As expected from the correlation seen in Figure 2(a), the variation as a function of distance from the MS is less pronounced for sources with values less than three times the MS value. Again, the data mainly follow the predicted trend from the 2-SFM model, also for sources in the transition to the starburst regime. The scatter for $t_{depl.}$ and $\mu_{mol.}$ is consistent with that seen at lower redshift used to predict the 2-SFM distribution. No obvious differences in the distribution of star-forming galaxies and galaxies potentially hosting an AGN can be seen for either quantity.

A clear link between μ_{gas} and sSFR has already been reported for local and high-redshift ($z < 3$) galaxies (e.g., Magdis et al. 2012; Saintonge et al. 2012; Bothwell et al. 2014; Dessauges-Zavadsky et al. 2015; Genzel et al. 2015). Our data suggests that the steep trend in $t_{depl.}$ with sSFR reported in the literature (e.g., Saintonge et al. 2011b; Dessauges-Zavadsky et al. 2015; Genzel et al. 2015) could at least partially be due to the transition to more starburst-like objects as indicated by the 2-SFM model predictions and the distribution of our few sources. As the transition region in the 2-SFM model encompasses about one order of magnitude and small errors on the sSFR determination could lead to large scatter, dedicated high-quality observations will be required to further test this.

3.2.2. Time Evolution

We compare the gas fraction $\mu_{gas} = M_{gas}/M_{\star}$ for our $z \sim 3.2$ sample to the predicted evolutionary trends from the 2-SFM model as well as literature values for larger samples (Bethermin et al. 2015; Genzel et al. 2015; Scoville et al. 2016) in Figure 3(a). Comparison to literature values from large samples shows that our results are in very good agreement with the findings of Genzel et al. (2015) and Bethermin et al. (2015). Our galaxies are also consistent with the average MS values of Scoville et al. (2016, their Table 2). The median value of our $z = 3.2$ sample of $\langle\mu_{gas}\rangle = 1.65^{+0.18}_{-0.19}$ (filled black triangle; uncertainties are 1σ error on the median) and the one compensated for the MS offset of our sample of $\langle\mu_{gas}\rangle_{comp} = 1.68^{+0.18}_{-0.19}$ (filled black star; uncertainties are 1σ error on the median) are consistent with the expected flattening of the $\mu_{gas}(z)$ curve at $z \gtrsim 2.5$ in the 2-SFM model (Sargent et al. 2014). The $z = 4.4$ data point of Scoville et al. (2016) falls slightly below the 2-SFM model line. As Scoville et al. (2016) also include non-detections in their average values (unlike Genzel et al. 2015 for the CO line measurements), this could point to a certain biasing of the results when only detections are considered (however, see the stacking data points from Bethermin et al. 2015) or be due to small number statistics (Scoville et al. 2016, include only six galaxies in their $z = 4.4$ measurement).

Our objects show a trend of gas fraction with specific SFR (as highlighted by the symbol color used in Figure 3 and expected from Section 3.2.1) covering more than one order of magnitude at $z \approx 3.2$. An exception are those galaxies that lie more than $2.5\times$ above the MS and do not follow the same trend due to their significantly different $t_{depl.}$ or star formation efficiency (SFE $= t_{depl.}^{-1}$) compared to MS galaxies. Our three AGN host galaxy candidates follow the overall trend of the remaining 42 galaxies.

This demonstrates how sensitive gas fraction measurements are on the range of SFRs sampled and illustrates how varying

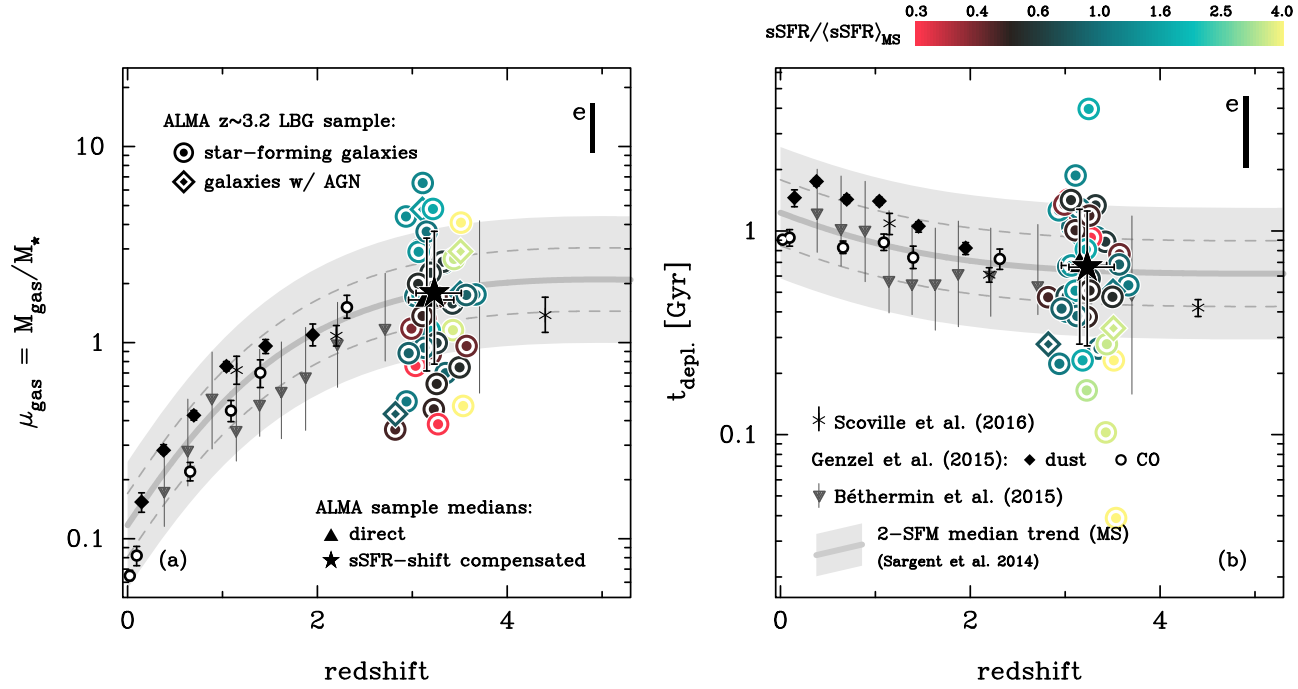

Figure 3. Redshift evolution of the (a) gas fraction $\mu_{\rm gas} = M_{\rm gas}/M_\star$ (left) and (b) depletion time $t_{\rm dep}$ (right). Our sample is color-coded according to the distance from the main sequence of star-forming galaxies with redder (greener) colors indicating objects below (above) the main sequence (see color bar in the top right) separated into star-forming galaxies (circles) and candidate AGN hosts (diamonds). The typical error bar of our objects marked by an "e" is indicated in the top right corner of each panel. The median values of our $z = 3.2$ sample are shown by large black triangles, while the median values compensated for the offset of our sample from the main sequence are given by the large black star symbols. The median trend predicted by the 2-SFM model for main-sequence galaxies (Sargent et al. 2014) is shown by the solid gray line, the dashed lines indicate the expected gas fraction (depletion time) for galaxies lying 1σ above or below the star-forming main sequence. Galaxies within 2σ of the average main-sequence locus are predicted to lie within the light gray band. Note that for low-z galaxies the contribution of atomic (H I) gas is not included in $M_{\rm gas}$. In addition, the average gas fraction derived from CO line observations (black open circles) and from stacked dust SEDs (black diamonds) at lower redshifts from the compilation by Genzel et al. (2015) is shown together with recent results using stacked dust SEDs in the COSMOS field (dark gray triangles, Bethermin et al. 2015) and sub-millimeter continuum measurements (black filled circles, Scoville et al. 2016).

selection criteria in different studies may produce discrepant results. Sources located below the MS of star-forming galaxies, i.e., with SFR lower than the median galaxy, will bias the gas fraction toward lower values. It also underlines the importance of a good (or at least consistent) determination of the SFR when comparing different surveys, or in other words the strong relation between $M_{\rm gas}$ and SFR strongly affects the interpretation of $\mu_{\rm gas}$. Our objects closest to the MS (color-coded dark green to black) typically lie closest to the expected value of $\mu_{\rm gas} \approx 2$, but they still show a significant scatter, suggesting that the intrinsic gas fraction for galaxies on the MS has a wide distribution. (Note that some of the scatter is also due to the fact that our galaxies sample a range of stellar masses with different average gas fractions; see Figure 4.) Larger samples are required to confirm this behavior.

Comparison of the gas depletion time $t_{\rm depl.}$ of our $z \sim 3.2$ sample to the 2-SFM model trend (Sargent et al. 2014) and literature values for larger samples is presented in Figure 3(b). The median direct and compensated values of our $z = 3.2$ sample of $\langle t_{\rm depl.}({\rm Gyr})\rangle = 0.68^{+0.07}_{-0.08}$ and $\langle t_{\rm depl.}({\rm Gyr})\rangle_{\rm comp} = 0.67^{+0.07}_{-0.08}$ (uncertainties are 1σ error on median) are fully consistent with the trends and values of Genzel et al. (2015) and Bethermin et al. (2015) which also follow the trend predicted by the 2-SFM model. According to data and model, $t_{\rm depl.}$ may approach a plateau of $t_{\rm depl.} \approx 600$ Myr for MS galaxies at $z \geqslant 3$. Again, the mean values of the MS galaxies from Scoville et al. (2016) are fully consistent with the other data, with the exception of the $z = 4.4$ data which tends toward values lower than predicted by the 2-SFM model, but still consistent within the expected scatter.

Our objects show no clear trend with specific SFR (as expected from Section 3.2.1) over almost two orders of magnitude at $z \approx 3.2$. An exception are the objects that lie more than $2.5\times$ above the MS that all exhibit depletion times of 300 Myr and less. It is interesting to note that our scatter is similar to that from the IR stacking analysis by Bethermin et al. (2015). This suggests that in addition to potential sample selection biases (fraction of starburst-like sources), a large intrinsic scatter could contribute to variations between different studies.

3.2.3. Trends with Stellar Mass

The gas fraction $\mu_{\rm gas}$ is slightly anti-correlated with stellar mass $M_\star$ for our $z = 3.2$ sample as shown in Figure 4. Our galaxies agree well with the general predicted trend by the 2-SFM model (Sargent et al. 2014), but they reveal an apparently steeper slope of $\mu_{\rm gas}(M_\star)$ that is likely an artifact created by our detection limit (see the long-dashed diagonal line in Figure 4).

At fixed stellar mass, galaxies with high gas fractions are on average expected to correspond to MS galaxies well above the mean MS locus according to the 2-SFM framework (see the colored band in the background of Figure 4). In Figure 4 we have colored our ALMA detections according to the actual sSFR-offset with respect to the MS. While there is an overall, broad agreement between expected and actual location of our data in Figure 4 (in the sense that high-sSFR galaxies lie above

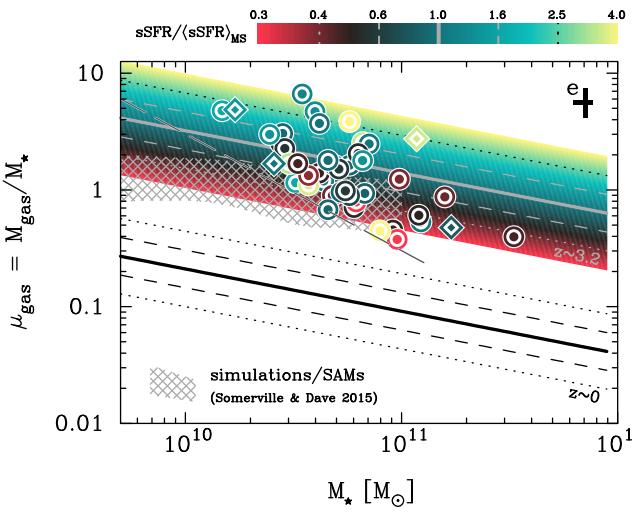

Figure 4. Gas fraction $\mu_{\rm gas}$ vs. stellar mass $M_\star$ at $z \sim 3.2$. Our $z = 3.2$ sample is color-coded based on distance from the main sequence of star-forming galaxies at $z \sim 3.2$ (see color bar on top of panel). Star-forming galaxies are indicated as circles, potential AGN hosts as diamonds. The typical error bar marked with an "e" is shown in the top right corner. The completeness limit (dark gray, dashed line) is dictated by our 3σ flux limit at $z \approx 3.2$, $\log(M_{\rm gas}[M_\odot]) = 10.48$. The predicted trend of gas fraction $\mu_{\rm gas}(M_\star)$ from 2-SFM (Sargent et al. 2014) is shown with the same color-coding as our data points, the solid gray line gives the median trend (for remaining lines see color bar). The corresponding lines in black show the same information for local galaxies at $z \sim 0$. The range of possible values predicted by cosmological simulations and semi-analytical models (SAMs) for MS galaxies compiled by Somerville & Davé (2015) is shown as the gray cross-hatched area. Note that for low-z galaxies the contribution of atomic (H I) gas is not included in $M_{\rm gas}$.

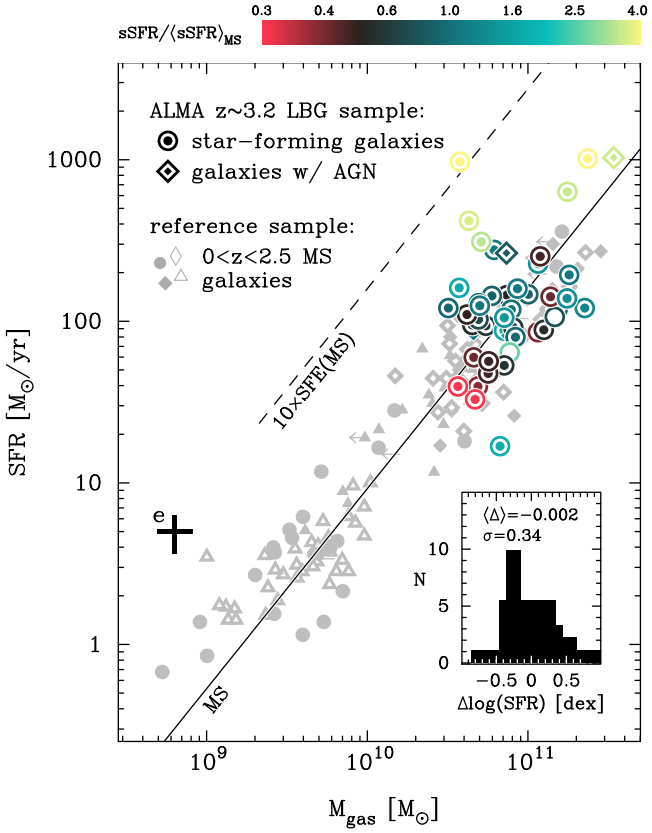

Figure 5. Star formation rate (SFR) vs. (molecular) gas mass. Our $z = 3.2$ sample (point color-coded based on distance from the main sequence of star-forming galaxies; color bar on top) scatters around the same power-law relation between SFR and gas mass occupied by $0 < z < 3$ main sequence galaxies (marked "MS"). For reference the location of high-efficiency starburst galaxies with ten-fold enhanced SFE (star formation efficiency) compared to MS galaxies is shown as well (black line labelled "10 × SFE(MS)"). Star-forming galaxies are shown as filled circles, while candidate AGN hosts as filled diamonds (open symbols are for $z < 2.8$ sources only). A representative error bar is indicated in the bottom left corner marked by an "e." The reference sample is from the compilation of Sargent et al. (2014) and comprises local to $z \sim 2.5$ galaxies on the main sequence. Note that for low-z galaxies the contribution of atomic (H I) gas is not included in $M_{\rm gas}$.

the average $\mu_{\rm gas}$ versus $M_\star$ trend and low-sSFR galaxies below), the fact that the color of the individual symbols and the background color scheme do not match up perfectly evidences a non-negligible scatter of the SFR versus $M_{\rm gas}$ relation. We will discuss this further in Section 4. Note that galaxies with $\mathrm{sSFR}/\langle\mathrm{sSFR}\rangle_{\rm MS} \gtrsim 3$ have gas fractions similar to the average MS galaxy with identical mass due to their enhanced star formation efficiency (or lower $t_{\rm depl.}$; see also Figure 2). It is interesting to note that most of the $\log(M_\star(M_\odot)) > 11$ galaxies are below the MS and also have the lower $\mu_{\rm gas}$ expected for objects with lower sSFR than the MS. However, the overall scatter is consistent with the range expected from the MS range probed by our galaxies.

Comparison of the trend from the 2-SFM model and our data to predicted relations from cosmological simulations and semi-analytical models compiled by Somerville & Davé (2015) shows that the observed gas fraction is typically a factor of $\sim$2× higher. The dependence of $\mu_{\rm gas}$ on $M_\star$ is probably stronger than seen in the cosmological models, though results appear to be very sensitive to the exact MS location of the sample studied. Our AGN host galaxies cover no preferred parameter space. A similar trend of $\mu_{\rm gas}$ is seen locally (Saintonge et al. 2011a; Bothwell et al. 2014) and also at higher redshift (e.g., Dessauges-Zavadsky et al. 2015; Genzel et al. 2015). No trend is obvious in our data when plotting $t_{\rm depl.}$ against $M_\star$. Since our data cover the same parameter space as the $z > 1$ star-forming galaxies compiled by Dessauges-Zavadsky et al. (2015, their Figure 9) this might be an effect of our limited stellar mass range probed.

4. NO CHANGE IN GLOBAL STAR FORMATION PROCESS OUT TO $z > 3$

The results from Section 3.2 for $t_{\rm depl.}$ and $\mu_{\rm gas}$ are (i) a redshift-independent dependence on sSFR and (ii) a flattening of the redshift evolution at $z \sim 3$. They imply that our $z \sim 3$ massive star-forming galaxies follow the relation between SFR and gas mass (i.e., the Schmidt–Kennicutt relation) established for lower redshift galaxies. This relation is one key ingredient in the 2-SFM prescription (see Sargent et al. 2014). Placing all our detections onto the SFR versus gas mass plane (Figure 5) shows that the $z \sim 3$ MS galaxies occupy the same space as lower redshift objects at $1.2 < z < 2.5$. The amplitude of the scatter of our sample restricted to $\pm$0.5 dex from the MS location (see inset in the bottom right corner) is about 1.7× larger than that observed for the reference MS samples (of $\approx$0.20 dex). It is interesting to note that there is a slight trend with MS location: galaxies well below the MS have a higher depletion time $t_{\rm depl.}$ (or lower star formation efficiency) than objects well above the MS that typically have a lower $t_{\rm depl.}$ (or higher star formation efficiency) than objects close to the MS. This is consistent with the trend seen in Figure 2(b). The larger

scatter in SFR is mainly caused by galaxies in the transition to starburst objects. The AGN host galaxies fall within the scatter of our star-forming galaxies. The mean MS values of Scoville et al. (2016) are also consistent with the location of our data points.

Our $z = 3.2$ MS galaxies follow the Schmidt–Kennicutt relation as determined through the fit by Sargent et al. (2014). This explicitly means that a single star formation prescription or "law" describes the relation between molecular gas mass and star formation activity out to $z > 3$—at least for MS galaxies. This was already concluded by Bethermin et al. (2015) from their IR stacking analysis.

The proposed redshift evolution of Saintonge et al. (2013) for $t_{\rm depl.}$ of $(1+z)^{\alpha}$ (their Equation (10)) of 0.36–0.17 Gyr (for their $\alpha \in [-1.0, -1.5]$) is inconsistent with our median $t_{\rm depl.}$ of 0.67 Gyr by a factor of $\gtrsim 2\times$. In the equilibrium framework developed for the bath tub or reservoir model, it is assumed $t_{\rm depl.} = t_{\rm H}\, M_{\rm star}^{-0.3}$ (Davé et al. 2012). As the literature and our data all probe roughly MS galaxies with similar stellar masses of a few times $10^{10}\,M_{\odot}$, the dependence should simplify to $t_{\rm depl.} \sim t_{\rm H} \sim t_{\rm dyn} \sim (1+z)^{-1.5}$ (e.g., Davé et al. 2012). Based on the data available it seems that this assumption is not valid or no longer valid at $z > 3$. For $\mu_{\rm gas}$ the situation is less clear as our preferred redshift-independent dependence of $\mu_{\rm gas}$ on sSFR from the 2-SFM framework gives values consistent with $\mu_{\rm gas} = 1/(1 + (t_{\rm depl.}(z)^{*}{\rm sSFR}(z))^{-1}))$ (see, e.g., Figure 11 of Saintonge et al. 2013). As this equation is one of the equilibrium relations proposed by Davé et al. (2012) this implies that sSFR might evolve less strongly with redshift than assumed, i.e., a shallower evolution than ${\rm sSFR} \sim (1+z)^{2.25}$ expected from cosmic inflow driven by gravitational infall (Davé et al. 2012) or the assumption of $t_{\rm dyn} \sim (1+z)^{-1.5}$ is not correct implying that the relation between galaxy and halo mass would evolve. Similarly, the trends for $\mu_{\rm gas}$ ($t_{\rm depl.}$) determined by Genzel et al. (2015) are not consistent at $z \approx 3.2$ with the measurements for our MS galaxies. In any case observations at redshifts higher than $z = 3$ are required for a more definite answer.

An interesting consequence of the fairly constant $t_{\rm depl.}$ and $\mu_{\rm gas}$ at $z > 2$ is the implication that the evolution in the cosmic SFR density at $z > 2$ for the high-mass systems studied here is then driven by the number density of such star-forming systems and not a change of the gas reservoir available. This is in contrast to the explanation for the observed strong decline in the cosmic star formation density at $z < 1$ where Karim et al. (2011) argue that a decline in the cold gas reservoir is the root cause as the number density of (massive) star-forming systems does not change. This might imply that we see the transition from the epoch of galaxy formation (at high z) to the epoch of star formation (at low z). The observed strong evolution of the UV luminosity function at $z > 4$ (e.g., Bouwens et al. 2015) suggests that the drop in the cosmic SFRD at these redshifts might be due to a combination of a decreasing number density of star-forming systems and an evolution of their luminosity. If the luminosity evolution of the high-mass systems is not as strong as inferred from the UV work, as suggested by Rowan-Robinson et al. (2016) based on an analysis of IR data, our original statement made for objects in the range $1.5 < z \lesssim 3$ can be extended to higher z.

Lagos et al. (2015) show the expected evolution of $\mu_{\rm gas}$ and $t_{\rm depl.}$ (their Figure 11) for two different prescriptions of H_2 formation applied to a set of the EAGLE cosmological simulations. Our observed values are about $3\times$ higher for both parameters than the predictions for MS galaxies with $\log(M_{\star}(M_{\odot})) > 9.7$ based on the simulations. Lagos et al. (2015) explain the drop in gas fraction and depletion time beyond $z \approx 3$ with a lower H_2 formation efficiency than at $z < 1$ due to lower gas phase metallicity and higher star formation surface densities. The mismatch might be due to the fact that our observations are probing a higher mass range implying a strong dependence of H_2 formation efficiency on stellar mass or that some physics are not sufficiently captured by the simulations.

Our data allows for a first glimpse on a potential evolution within the MS. Tacchella et al. (2016) observe in their simulations the following trend: galaxies above the MS compact their gas reservoir leading to higher SFR, higher $\mu_{\rm gas}$ and shorter $t_{\rm depl.}$. Once the (central) gas reservoir is exhausted, galaxies drop below the MS with lower SFR, lower $\mu_{\rm gas}$, and longer $t_{\rm depl.}$. Our data are consistent with an MS trend in $\mu_{\rm gas}$, however, an MS trend for $t_{\rm depl.}$ is only evident once objects in transition to starbursts are taken into account. Thus to test this scenario further a larger sample and, more critically, morphological information on the gas reservoir, i.e., its size, are required.

In summary our ALMA observations of the gas mass in 45 $z \approx 3.2$ massive MS galaxies suggest that a single relation between gas mass and SFR is sufficient to explain the evolution of the gas fraction and depletion out to $z > 3$ for normal star-forming galaxies. As already pointed out earlier, our methods account for the contribution of molecular and atomic gas, while most of the other methods are calibrated for the molecular component only. Given the close agreement between derived gas masses of our method and the calibration of Scoville et al. (2016) for our galaxies as well as the expected low atomic gas content at $z > 3$ (e.g., Obreschkow & Rawlings 2009; Popping et al. 2014; Lagos et al. 2011), we do not expect that this introduces large uncertainties for our sample galaxies.

5. SUMMARY AND CONCLUSIONS

We present 45 ALMA continuum detections of massive MS galaxies (with $\langle \log(M_{\star}(M_{\odot}) \rangle = 10.7$ and $\langle \log({\rm sSFR}({\rm yr}^{-1}) \rangle = -8.6$) at $z \approx 3.2$ in the COSMOS field. Conversation of the rest-frame sub-millimeter continuum luminosity to gas mass allowed us to derive the gas fraction $\mu_{\rm gas} = M_{\rm gas}/M_{\star}$ and gas depletion time $t_{\rm depl.} = M_{\rm gas}/{\rm SFR}$. Our data points are consistent with literature values reported at lower and higher redshifts for these parameters. Our median values of $\langle \mu_{\rm gas} \rangle = 0.68$ and $\langle t_{\rm depl.} \rangle = 0.68$ Gyr imply a flattening of the redshift trends beyond $z \approx 2$, inconsistent with the expected evolution for a strong dependence on dynamical time. The surprisingly good agreement with the predicted trends from the 2-SFM framework suggest that these analytic prescriptions are a good representation of the evolution of $\mu_{\rm gas}$ and $t_{\rm depl.}$—at least for massive MS galaxies out to $z \sim 4$. It further implies that the relation between SFR and gas mass is constant and does not evolve over time.

We warmly thank the German ALMA ARC node for their excellent support for this project and R. Somerville for providing the information on the simulation predictions for our redshift range of interest. We also thank the referee for constructive comments. E.S. acknowledges fruitful discussions with R. Somerville, R. Feldmann, N.Z. Scoville, N. Bouché,

and C. de Breuck that helped to significantly focus the paper. B.G. gratefully acknowledges the support of the Australian Research Council as the recipient of a Future Fellowship (FT140101202). A.K. acknowledges support by the Collaborative Research Council 956, sub-project A1, funded by the Deutsche Forschungsgemeinschaft (DFG). Support for B.M. was provided by the DFG priority program 1573 "The physics of the interstellar medium." V.S. acknowledges funding from the European Union's Seventh Framework program under grant agreement 337595 (ERC Starting Grant, "CoSMass"). This paper makes use of the following ALMA data: ADS/JAO.ALMA#2013.1.00151.S. ALMA is a partnership of ESO (representing its member states), NSF (USA), and NINS (Japan), together with NRC (Canada), NSC, and ASIAA (Taiwan), and KASI (Republic of Korea), in cooperation with the Republic of Chile. The Joint ALMA Observatory is operated by ESO, AUI/NRAO, and NAOJ. Based on data obtained with the European Southern Observatory Very Large Telescope, Paranal, Chile, under Large Program 185.A-0791.

Facility: ALMA.

REFERENCES

Arnouts, S., Cristiani, S., Moscardini, L., et al. 1999, MNRAS, 310, 540
Arnouts, S., Moscardini, L., Vanzella, E., et al. 2002, MNRAS, 329, 355
Bethermin, M., Daddi, E., Magdis, G., et al. 2015, A&A, 573, A113
Bethermin, M., Kilbinger, M., Daddi, E., et al. 2014, A&A, 567, A103
Bothwell, M. S., Wagg, J., Cicone, C., et al. 2014, MNRAS, 445, 2599
Bouwens, R. J., Illingworth, G. D., Oesch, P. A., et al. 2015, ApJ, 803, 34
Bruzual, G., & Charlot, S. 2003, MNRAS, 344, 1000
Carilli, C. L., & Walter, F. 2013, ARA&A, 51, 105
Civano, F., Marchesi, S., Comastri, A., et al. 2016, ApJ, 819, 62
da Cunha, E., Charlot, S., & Elbaz, D. 2008, MNRAS, 388, 1595
Davé, R., Finlator, K., & Oppenheimer, B. D. 2012, MNRAS, 421, 98
Dessauges-Zavadsky, M., Zamojski, M., Schaerer, D., et al. 2015, A&A, 577, A50
Draine, B. T., & Li, A. 2007, ApJ, 657, 810
Genzel, R., Tacconi, L. J., Lutz, D., et al. 2015, ApJ, 800, 20
Groves, B. A., Schinnerer, E., Leroy, A., et al. 2015, ApJ, 799, 96
Heinis, S., Buat, V., Béthermin, M., et al. 2014, MNRAS, 437, 1268
Hildebrand, R. H. 1983, QJRAS, 24, 267
Ilbert, O., Arnouts, S., McCracken, H. J., et al. 2006, A&A, 457, 841
Ilbert, O., McCracken, H. J., Le Fevre, O., et al. 2013, A&A, 556, 55
Karim, A., Schinnerer, E., Martinez-Sansigre, A., et al. 2011, ApJ, 730, 61
Karim, A., Swinbank, A. M., Hodge, J. A., et al. 2013, MNRAS, 432, 2
Kennicutt, R. C., Calzetti, D., Aniano, G., et al. 2011, PASP, 123, 1347
Kewley, L. J., Dopita, M. A., Leitherer, C., et al. 2013, ApJ, 774, 100
Kewley, L. J., Zahid, H. J., Geller, M. J., et al. 2015, ApJL, 812, L20
Lacy, M., Petric, A. O., Sajina, A., et al. 2007, AJ, 133, 186
Lagos, C. d. P., Baugh, C. M., Lacey, C. G., et al. 2011, MNRAS, 418, 1649
Lagos, C. d. P., Crain, R. A., Schaye, J., et al. 2015, MNRAS, 452, 3815
Laigle, C., McCracken, H. J., Ilbert, O., et al. 2016, ApJS, 224, 24
Le Fevre, O., Tasca, L. A. M., Cassata, P., et al. 2015, A&A, 576, A79
Le Floc'h, E., Aussel, H., Ilbert, O., et al. 2009, ApJ, 703, 222
Lee, J. C., Gil de Paz, A., Kennicutt, R. C., et al. 2010, ApJS, 192, 6
Leroy, A. K., Bolatto, A., Gordon, K., et al. 2011, ApJ, 737, 12
Lilly, S. J., Fevre, O. L., Renzini, A., et al. 2007, ApJS, 172, 70
Lutz, D., Poglitsch, A., Altieri, B., et al. 2011, A&A, 532, A90
Magdis, G. E., Daddi, E., Sargent, M., et al. 2012, ApJL, 758, L9
Magdis, G. E., Rigopoulou, D., Huang, J. S., & Fazio, G. G. 2010, MNRAS, 401, 1521
Magnelli, B., Lutz, D., Saintonge, A., et al. 2014, A&A, 561, A86
Magnelli, B., Popesso, P., Berta, S., et al. 2013, A&A, 553, A132
Maiolino, R., Nagao, T., Grazian, A., et al. 2008, A&A, 488, 463
McCracken, H. J., Milvang-Jensen, B., Dunlop, J., et al. 2012, A&A, 544, A156
Muzzin, A., Marchesini, D., Stefanon, M., et al. 2013, ApJS, 206, 8
Noeske, K. G., Weiner, B. J., Faber, S. M., et al. 2007, ApJL, 660, L43
Obreschkow, D., & Rawlings, S. 2009, ApJL, 696, L129
Onodera, M., Carollo, C. M., Lilly, S., et al. 2016, ApJ, 822, 42
Popping, G., Somerville, R. S., & Trager, S. C. 2014, MNRAS, 442, 2398
Rowan-Robinson, M., Oliver, S., Wang, L., et al. 2016, MNRAS, 461, 1100
Saintonge, A., Kauffmann, G., Kramer, C., et al. 2011a, MNRAS, 415, 32
Saintonge, A., Kauffmann, G., Wang, J., et al. 2011b, MNRAS, 415, 61
Saintonge, A., Lutz, D., Genzel, R., et al. 2013, ApJ, 778, 2
Saintonge, A., Tacconi, L. J., Fabello, S., et al. 2012, ApJ, 758, 73
Santini, P., Maiolino, R., Magnelli, B., et al. 2014, A&A, 562, A30
Sargent, M. T., Daddi, E., Béthermin, M., et al. 2014, ApJ, 793, 19
Schreiber, C., Pannella, M., Elbaz, D., et al. 2015, A&A, 575, A74
Scoville, N., Aussel, H., Sheth, K., et al. 2014, ApJ, 783, 84
Scoville, N., Sheth, K., Aussel, H., et al. 2016, ApJ, 820, 83
Somerville, R. S., & Davé, R. 2015, ARA&A, 53, 51
Speagle, J. S., Steinhardt, C. L., Capak, P. L., & Silverman, J. D. 2014, ApJS, 214, 15
Steinhardt, C. L., Speagle, J. S., Capak, P., et al. 2014, ApJL, 791, L25
Tacchella, S., Dekel, A., Carollo, C. M., et al. 2016, MNRAS, 457, 2790
Tan, Q., Daddi, E., Magdis, G., et al. 2014, A&A, 569, A98
Tasca, L. A. M., Le Fevre, O., Hathi, N. P., et al. 2015, A&A, 581, A54
Tomczak, A. R., Quadri, R. F., Tran, K.-V. H., et al. 2016, ApJ, 817, 118
Troncoso, P., Maiolino, R., Sommariva, V., et al. 2014, A&A, 563, A58